# Characterization of an elastic target in a shallow water waveguide by decomposition of the time-reversal operator

Franck D. Philippe,[a) Claire Prada, Julien de Rosny, Dominique Clorennec,
Jean-Gabriel Minonzio, and Mathias Fink
*Laboratoire Ondes et Acoustique, Université Denis Diderot Paris 7, UMRS CNRS 7587, ESPCI, 10 rue Vauquelin, 75231 Paris Cedex 05, France*

This paper reports the results of an investigation into extracting of the backscattered frequency signature of a target in a waveguide. Retrieving the target signature is difficult because it is blurred by waveguide reflections and modal interference. It is shown that the decomposition of the time-reversal operator method provides a solution to this problem. Using a modal theory, this paper shows that the first singular value associated with a target is proportional to the backscattering form function. It is linked to the waveguide geometry through a factor that weakly depends on frequency as long as the target is far from the boundaries. Using the same approach, the second singular value is shown to be proportional to the second derivative of the angular form function which is a relevant parameter for target identification. Within this framework the coupling between two targets is considered. Small scale experimental studies are performed in the 3.5 MHz frequency range for 3 mm spheres in a 28 mm deep and 570 mm long waveguide and confirm the theoretical results. © 2008 Acoustical Society of America. [DOI: 10.1121/1.2939131]

## I. INTRODUCTION

In a shallow water waveguide, active detection and characterization of a target is an active field of research. Recent developments in sonar technology are very promising for target detection but efficient techniques to characterize those targets with conventional Sonar techniques remain scarce. A major difficulty comes from the dispersive nature of the waveguide. Indeed an impulse signal evolves into a long wave packet before reaching the target and then the backscattered wave is once again modified by the transfer function of the waveguide. As a consequence, the frequency fluctuations of a target's response are dominated by the boundary reflections and highly depend on the receiver depth.[1,2] Therefore, in shallow water, even if the backscattered signals are free of bottom reverberation, the extraction of the target's signature is very challenging.

To overcome this problem, the most common method is to deconvolve the transfer function of the waveguide. However, it is well known that the deconvolution problem for one transducer is ill posed; in other words, the solution is nonunique for a given set of data. In order to solve this problem, a solution is to use a vertical source-receiver array (SRA) that spans the whole water column. For instance, Mignerey and co-workers successfully demonstrated passive multichannel deconvolution using estimated boundary conditions and environmental data in an oceanic waveguide.[3,4]

Several studies address the direct or inverse problem of target scattering in a waveguide using a SRA. In particular, the scattering from an extended object is discussed by Yang and Yates in terms of mode coupling between the incident field and the scattered field.[5] They show that the use of a vertical SRA is necessary to acquire a large set of modes in order to extract the angular dependence of the scattered field.

In this paper, a method is proposed to circumvent the complexity of the acoustic response of the propagating medium by applying the decomposition of the time-reversal operator (DORT) method with a vertical SRA. In a waveguide, this method, like other time reversal techniques,[6–8] takes advantage of the multipath propagation to achieve high resolution detection and focusing. It requires the acquisition of the full interelement response matrix of the SRA. From the singular value decomposition (SVD) of the array response matrix, a set of singular vectors and singular values is determined. The singular vectors are eigenvectors of the time-reversal operator (TRO) and lead to the localization of pointlike scatterers. It was shown that in a waveguide, the transmission of eigenvectors of the TRO allows selective focusing on different pointlike targets.[9,10] This decomposition is also a means to separate the echo of a target from ground reverberation[11] and it was used to achieve reverberation focusing and nulling.[12,13] Recent at sea experiments confirm the efficiency of the DORT method for detection and focusing in a shallow water environment.[14,15] However, the aforementioned studies only considered isotropic scatterers.

Until now, application of the DORT method to elastic anisotropic scatterers (cylinders or spheres) has been studied in free space by Chambers and co-worker[16,17] and Minonzio *et al.*[18,19] It was shown that the frequency dependence of the singular values permits characterizing an elastic target. In fact, the first singular value is proportional to the backscattering form function used in underwater acoustics.[20]

This paper presents the results of the study into the effect of the waveguide on the singular values of the array response matrix and for the particular case of a Pekeris waveguide, analytical results are presented. It is organized as

---

a)Electronic mail: franck.philippe@espci.fr

follows: first in Sec. II a theory is derived, showing that for one isotropic scatterer, if the array spans the whole water column, the backscattering form function of the target is given by the first singular value despite the reflections from the boundaries. Then this result is generalized for two scatterers and for large scatterers.

Finally, in Sec. III, ultrasonic waveguide experiments mimicking at sea underwater experiments are presented that confirm the theoretical results.

## II. EXTRACTION OF THE SIGNATURE OF AN ISOTROPIC SCATTERER: THEORY

When using the DORT method, multiple paths from one target to the array are exploited allowing high resolution focusing. The resolution is increased because the effective aperture of the array in the waveguide is similar to a larger aperture virtual array in free space. In 1987, Ingenito[2] derived an expression for the acoustic field scattered by an elastic sphere using a normal mode decomposition. In the following, the extraction of the target signature is derived in a similar manner. Furthermore, it is demonstrated that the first singular value of the array response matrix is proportional to the target form function, that is to say, the monostatic frequency response in free space.

### A. One isotropic scatterer

The analysis is performed in the frequency domain and for simplicity, the frequency dependence is kept implicit. The vector $\mathbf{h}_s$ has its $i$th element $[\mathbf{h}_s]_i$ equal to the Green's function between the scatterer at position $\mathbf{r}_s$ of cylindrical coordinates $(z_s, r_s)$ and the transducer number $i$ at position $\mathbf{r}_i$ of cylindrical coordinates $(z_i, r_i)$. Thanks to the reciprocity principle, the vector describing the propagation for the wave from the array to the scatterer is given by the transpose $\mathbf{h}_s$ denoted $\mathbf{h}_s^t$.

Let us first consider an isotropic scatterer characterized by $S(0)$, the scattering coefficient. The expression of the array response matrix $\mathbf{K}$ is

$$\mathbf{K} = \mathbf{h}_s S(0) \mathbf{h}_s^t. \tag{1}$$

The matrix $\mathbf{K}$ is symmetrical and its rank equals 1 by construction. Thus the SVD of $\mathbf{K}$ is written as

$$\mathbf{K} = \mathbf{U}_1 \sigma_1 \mathbf{V}_1^\dagger, \tag{2}$$

where $\sigma_1$ is the unique singular value larger than 0, and $\mathbf{U}_1$ and $\mathbf{V}_1$ are the normalized singular vectors. The Hermitian transpose is noted.[†]

By identification of Eq. (1) with Eq. (2), the first singular value is $\sigma_1 = |S(0)| \|\mathbf{h}_s\|^2$. Hence, the singular value does not only depend on the scatterer form function but also on the propagation phenomena through $\|\mathbf{h}_s\|$. Using the Green's functions $G$, the norm of $\mathbf{h}_s$ is given by

$$\|\mathbf{h_s}\|^2 = \sum_{i=1}^{N} |G(z_i, z_s, r_s - r_i)|^2. \tag{3}$$

In a waveguide that is range independent, the Green's function only depends on three position variables, the depth of
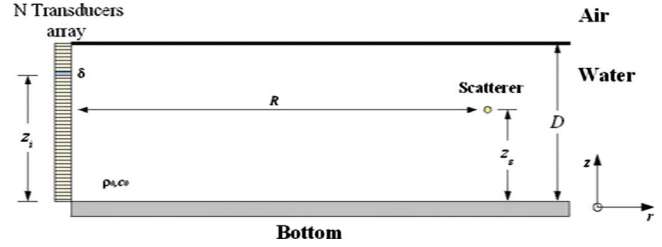


FIG. 1. (Color online) Geometry of the experiment and parameters.

the source $z_i$, the depth of the scatterer $z_s$, and the range between the source and the probed position $R = |r_s - r_i|$ (Fig. 1). Assuming that the SRA samples sufficiently well the water column, the discrete sum in Eq. (3) is replaced by a continuous integral as follows:

$$\|\mathbf{h_s}\|^2 = \sum_{i=1}^{N} |G(z_i, z_s, r_s - r_i)|^2 \approx \frac{1}{\delta} \int_0^D |G(z_i, z_s, r_s - r_i)|^2 dz, \tag{4}$$

where $\delta$ is the array pitch and $D$ is the water depth. The Green's function can be decomposed into the normal modes of the waveguide, i.e.,

$$G(z, z_s, R) = \frac{i}{4\rho} \sum_{m=0}^{\infty} \Psi_m(z_s) \Psi_m(z) H_0^{(1)}(k_{rm} R), \tag{5}$$

where $\Psi_m(z)$ is the normal mode associated with the vertical wave number $k_{zm}$. For an isospeed problem, the radial wave number $k_{rm}$ is linked to $k_0$ and $k_{zm}$ by the relation $k_{rm} = \sqrt{k_0^2 - k_{zm}^2}$. When $R$ is large enough, replacement of the Hankel function of first order $H_0^{(1)}$ by its asymptotic approximation transforms the Green's function expression into

$$G(z, z_s, R) \approx \frac{i}{\rho\sqrt{8\pi R}} e^{-i\pi/4} \sum_{m=0}^{\infty} \Psi_m(z_s) \Psi_m(z) \frac{e^{ik_{rm}R}}{\sqrt{k_{rm}}}. \tag{6}$$

In a Pekeris waveguide, the impedance mismatch between the water and the bottom is finite. One can show that $k_{rm}$ is purely real only when $k_b < k_{rm} < k_0$, where $k_b$ is the bottom wave number and $k_0$ is the water wave number. In other words, when the propagation angle $\theta_m$ with the horizontal line associated with the mode $m$ $[\cos(\theta_m) = k_{rm}/k_0]$ is lower than the Brewster angle, $\theta_b$ $[\cos(\theta_b) = c_0/c_b]$, the mode propagates with very little attenuation (other than geometrical spreading loss). For $\theta_m > \theta_b$, modes leak into the sea bottom and they decrease exponentially with range.[21] Moreover, the SRA transducers are not pointlike and thus have a directivity angle denoted $\theta_d$. As a consequence, the transducer array is not sensitive to modes with $\theta_d < \theta_m$.

Finally, at long range, only the modes with $\theta_m < \theta_{max}$ $[\theta_{max} = \min(\theta_d, \theta_b)]$ contribute to the field recorded by the array. The Green's function is well approximated by replacing the infinite sum by a finite sum with a maximum index equal to $M-1$, where $M-1$ is such that $k_{rM1} = k_0 \cos(\theta_{max})$.

Using Eqs. (4) and (6) and the orthogonality property between normal modes, the norm of $\mathbf{h}_s$ is given by

$$\|\mathbf{h}_s\|^2 = \frac{1}{\delta\rho 8\pi R}\sum_{m=0}^{M-1}\frac{\Psi_m^2(z_s)}{k_{rm}}. \tag{7}$$

Hence from the last equation, the expression for the singular value of a pointlike scatterer is deduced,

$$\sigma_1 = \frac{|S(0)|}{\rho 8\pi Rk_0\delta}\sum_{m=0}^{M-1}\frac{\Psi_m^2(z_s)}{\sqrt{1-\sin^2(\theta_m)}}, \tag{8}$$

where $k_0$ is the intrinsic wave number given by $k_0 = 2\pi f/c$ and $\sin(\theta_m) = k_{zm}/k_0$.

In the case of a Pekeris waveguide, the expressions for the lossless modes $\Psi_m$ are well approximated by[21]

$$\Psi_m(z) = \sqrt{\frac{2\rho}{D}}\sin(k_{zm}z) \quad\text{and}\quad k_{zm} = \frac{\pi}{2D} + \frac{m\pi}{D}.$$

Replacing $\Psi_m(z)$ by the above expression, Eq. (8) becomes

$$\sigma_1 = \frac{|S(0)|}{4\pi RDk_0\delta}\sum_{m=0}^{M-1}\frac{\sin^2(k_{zm}z_s)}{\sqrt{1-\sin^2(\theta_m)}}. \tag{9}$$

In most experiments, $\theta_{max}$ is small and as $\theta_m > \theta_{max}$, a series expansion in terms of $\sin^2(\theta_m)$ is justified,

$$\sigma_1 = \frac{|S(0)|}{4\pi RDk_0\delta}\sum_{m=0}^{M-1}\sin^2(k_{zm}z_s)\left(1+\frac{\sin^2(\theta_m)}{2}+\cdots\right). \tag{10}$$

Keeping only the first term of the expansion, $\sigma_1$ is approximated by

$$\sigma_1 \approx \frac{|S(0)|}{4\pi RDk_0\delta}\sum_{m=0}^{M-1}\sin^2(k_{zm}z_s). \tag{11}$$

Substitution of the expression of $k_{zm}$ in Eq. (11) yields (Appendix A)

$$\sigma_1 \approx \frac{|S(0)|}{4\pi RDk_0\delta}\frac{M}{2}\left[1-\frac{1}{M}f_M\left(\frac{z_s}{D}\right)\right], \tag{12}$$

where $f_M(\xi) = \cos(\pi M\xi)[\sin(\pi M\xi)/\sin(\pi\xi)]$.

The function $f_M$ is maximum at $\xi=0$ $[f_M(0)=M]$ and minimum at $\xi=1$ $[f_M(1)=-M]$. Between these two extremes, the function is close to 0. The characteristic width (first zero) $\delta\xi$ associated with the two extremes equals $1/M$.

The expression for $\sigma_1$ deserves several comments. First, when the target is far from the boundaries, the second term in Eq. (12) is negligible so that $\sigma_1$ is constant with depth and equal to $|S(0)|M/(8\pi RDk_0\delta)$. Considering that $M=2\sin(\theta_{max})D/\lambda$, the minimum distance between the target and the boundaries can be written as $\Lambda=\lambda/2\sin(\theta_{max})$ and as $\theta_{max}$ weakly depends on frequency, the only frequency dependence of $\sigma_1$ comes from $|S(0)|$. Note that this result can be generalized to other types of waveguides, provided $k_{zm}$ is roughly proportional to $m$. Second, when the target is close to the surface, $\sigma_1$ decreases until it reaches 0. Indeed, due to the pressure release boundary condition, the pressure field is zero close to the surface and the target is invisible. In contrast, close to the bottom, the pressure field is maximum and the singular value is twice its value in the middle of the
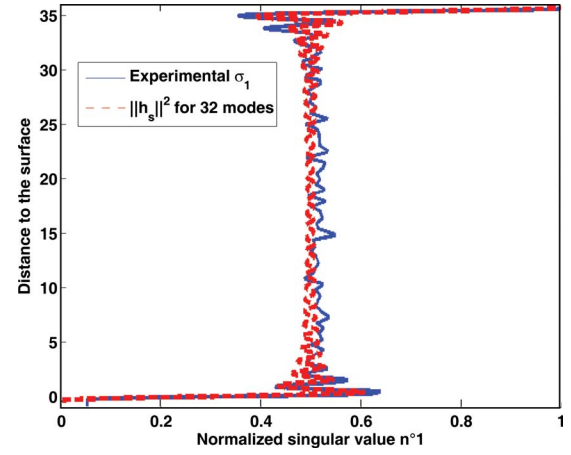


FIG. 2. (Color online) Comparison between the first singular value $\sigma_1$ given by Eq. (11) and the experimental singular value measured by Mordant et al. (Ref. 9) as a function of the target's depth for a frequency of 1.5 MHz.

waveguide. This analytical formulation of the first singular value is in good agreement with the experimental results presented by Mordant et al.[9] Indeed, in this paper, the authors applied the DORT method to the detection of a 0.2 mm diameter nylon wire in a waveguide. The experiment was done with a 60-element transducer array with a central frequency of 1.5 MHz and an array pitch of 0.58 mm. The water waveguide was delimited by air and a steel bottom, it was 35 mm deep and the nylon wire was at range 400 mm. The wire was moved from the bottom to the surface, and for each position, the array response matrix was recorded, and the first singular value was plotted as a function of depth (Fig. 2).

Mordant et al. proposed a numerical model using the virtual images of the array with respect to the waveguide interfaces. They found that the experimental results were well fitted considering only the first 11 reflections. For such a number of reflections, Eq. (D4) in Appendix D gives a maximum of 32 modes. In Fig. 2, the first singular value given by Eq. (11) is plotted for $M=32$. The agreement between theoretical and experimental values is excellent.

## B. Two isotropic scatterers

The case of two pointlike and isotropic scatterers can now be addressed. Neglecting multiple scattering, the array response matrix can be written as the sum of the transfer matrices of each scatterer alone[22]

$$\mathbf{K} = \mathbf{h}_{s1}S_1(0)\mathbf{h}_{s1}^t + \mathbf{h}_{s2}S_2(0)\mathbf{h}_{s2}^t, \tag{13}$$

where $\{\mathbf{h}_{s1}\}_i = G(z_{s1},z_i,r_{s1}-r_i)$ and $\{\mathbf{h}_{s2}\}_i = G(z_{s2},z_i,r_{s2}-r_i)$.

A coupling between the two scatterers will introduce complications in the singular value decomposition of $K$. Its formulation will not be as easily deduced as the two vectors $\mathbf{h}_{s1}$ and $\mathbf{h}_{s2}$ will not be orthogonal anymore. As a consequence, the same approach can be used on each term only if the inner product $\mathbf{h}_{s2}^\dagger\mathbf{h}_{s1}$ is small enough to be negligible. This product can be calculated using the modal decomposition

J. Acoust. Soc. Am., Vol. 124, No. 2, August 2008

Philippe et al.: Elastic target characterization in shallow water     781

$$\mathbf{h}_{s2}^{\dagger}\mathbf{h}_{s1} = \frac{1}{\delta 4\pi R}\sum_{m=0}^{M-1}\frac{\Psi_m(z_{s1})\Psi_m(z_{s2})}{k_{rm}}e^{ik_{rm}(R_1-R_2)}. \quad (14)$$

Here, for simplicity, we assume that the two targets are at the same range ($R_1=R_2$). The inner product becomes

$$\mathbf{h}_{s2}^{\dagger}\mathbf{h}_{s1} \approx \frac{1}{\delta 4\pi Rk_0}\sum_{m=0}^{M-1}\Psi_m(z_{s1})\Psi_m(z_{s2}). \quad (15)$$

In Appendix B, we show that this product can be expressed in terms of the $f_M$ function

$$\mathbf{h}_{s2}^{\dagger}\mathbf{h}_{s1} \approx \frac{1}{\delta\rho 8\pi Rk_0}\left[f_M\left(\frac{z_1+z_2}{2D}\right) - f_M\left(\frac{z_1-z_2}{2D}\right)\right]. \quad (16)$$

Far from the boundaries, the coupling between the two targets can be neglected when $|z_2-z_1|>D/M$. However, again $M\sim 2\sin(\theta_{max})D/\lambda$ so $|z_2-z_1|>\Lambda$. This expression is consistent with the Rayleigh criterion taking into account the angular aperture $2\theta_{max}$. Nevertheless, the modal approach is more general because it is still valid near the boundaries.

## C. One extended axisymmetrical scatterer

An extended scatterer is characterized by a frequency dependent form function $S$ depending on the incoming angle $\theta_1$ and the outgoing angle $\theta_2$. For axisymmetric scatterers at one frequency, the form function only depends on the angle difference $\theta_2-\theta_1$ and is even. Assuming small angles one can write the second order Taylor expansion as

$$S(\theta_2-\theta_1) = \left[S(0) + \frac{(\theta_2-\theta_1)^2}{2}S''(0)\right]. \quad (17)$$

A plane wave is written as $\varphi_\theta(r,z) = \exp[-ik_0(\sin\theta z + \cos\theta r)]$, where $k_0$ is the wave number, $r$ is the range, and $z$ is the height. Introduction of the following derivation operators $\partial_z^L$ and $\partial_z^R$ such that $\partial_z^L(\varphi,\psi)=(\partial\varphi/\partial z)\psi$ and $\partial_z^R(\varphi,\psi)=(\partial\psi/\partial z)\varphi$ will be useful for the following derivation. Indeed using those operators on two plane waves $\phi_{\theta_1}$ and $\phi_{\theta_2}$ yields $\partial_z^L(\varphi_{\theta_1},\varphi_{\theta_2})=-ik_0\sin\theta_1\varphi_{\theta_1}\varphi_{\theta_2} \approx -ik_0\theta_1\varphi_{\theta_1}\varphi_{\theta_2}$ and similarly $\partial_z^R(\varphi_{\theta_1},\varphi_{\theta_2}) \approx -ik_0\theta_2\varphi_{\theta_1}\varphi_{\theta_2}$. Here the small angle approximation was made. As a consequence, Eq. (17) can be expressed in terms of $\varphi_{\theta_1}$, $\varphi_{\theta_2}$ instead of $\theta_1$, $\theta_2$,

$$S(\theta_2-\theta_1) = S(0)\varphi_{\theta_1}\varphi_{\theta_2}|_{z,r=0} - S''(0)$$
$$\times \frac{(\partial_z^L-\partial_z^R)^2}{2k_0^2}(\varphi_{\theta_1},\varphi_{\theta_2})\bigg|_{z,r=0}. \quad (18)$$

As this approximation is valid for all pairs of plane waves with small angles, it can be generalized to any pair of fields satisfying the paraxial approximation. So, assuming that the Green's function $\{\mathbf{h}_s\}_i$ from any of the transducers to the scatterer center satisfies the parabolic approximation, the array response matrix can be written as
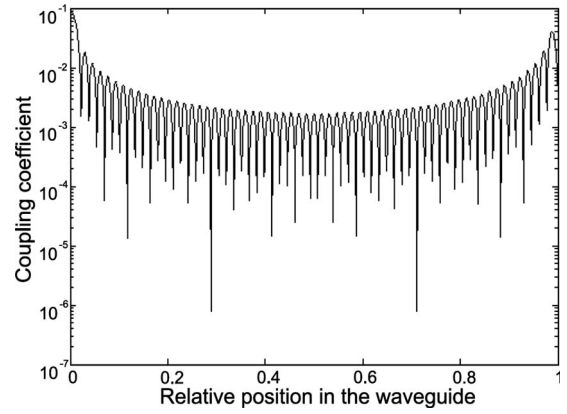


FIG. 3. Scalar product $\Sigma$ of the first two singular vectors of the array response matrix $\mathbf{K}$ with respect to the relative depth position of the target in the waveguide.

$$\mathbf{K} = S(0)\mathbf{h}_s\mathbf{h}_s^t + \frac{S''(0)}{k_0^2}\partial_z\mathbf{h}_s\partial_z\mathbf{h}_s^t - \frac{S''(0)}{2k_0^2}[\mathbf{h}_s(\partial_z^2\mathbf{h}_s^t)$$
$$+ (\partial_z^2\mathbf{h}_s)\mathbf{h}_s^t]. \quad (19)$$

Finally, assuming that $\mathbf{h}_s^{\dagger}\cdot\partial_z\mathbf{h}_s\approx 0$, $\partial_z^2\mathbf{h}_s^{\dagger}\cdot\partial_z\mathbf{h}_s\approx 0$, and $\|\mathbf{h}_s\|\gg\|\partial_z^2\mathbf{h}_s\|/k_0^2$ (paraxial approximation), the first singular vector is $\mathbf{V}_1=\mathbf{h}_s/\|\mathbf{h}_s\|$ with the singular value $\sigma_1=S(0)\|h\|^2$ and the second singular vector is $\mathbf{V}_2=\partial_z\mathbf{h}_s/\|\partial_z\mathbf{h}_s\|$ with the singular value $\sigma_2=S''(0)\|\partial_z h\|^2/k_0^2$.

Hence the two first singular values in the waveguide are simply related to the backscattering form function $S(0)$ and its second derivative $S''(0)$ only when the scalar product

$$\Sigma = \frac{\mathbf{h}_s^{\dagger}}{\|\mathbf{h}_s\|}\cdot\frac{\partial_z\mathbf{h}_s}{\|\partial_z\mathbf{h}_s\|} \quad (20)$$

is small compared to 1.

An analytical expression for $\Sigma$ is derived in Appendix C. The coupling term $\Sigma$ is plotted with respect to the scatterer depth in Fig. 3. This coupling decreases from the maximum near the boundaries (about 10%) to the minimum (about 0.2%) over a characteristic distance given by $\Lambda$. These results are consistent with the study made by Gaunaurd and Huang for a sphere near a hard flat boundary.[20]

In Appendix D the ratio between the singular values obtained with and without the waveguide interfaces shows that the waveguide enhances the first singular value by a factor of $2R\sin(\theta_{max})/D$ which is the number of reflections from the boundaries while the enhancement reaches $[2R\sin(\theta_{max})/D]^3$ for the second singular value.

This result shows that the second singular value can be a good complementary parameter for the identification of a target in a waveguide.

## III. EXPERIMENTAL RESULTS AND DISCUSSION

### A. Experimental setup

The data have been obtained with an array made of 64 transducers working at 3.5 MHz using 1 $\mu$s pulses ($\lambda$ = 0.43 mm). The array pitch is $\delta=0.417$ mm leading to an array aperture equal to 26.7 mm. The waveguide interfaces are air/water and water/Plexiglas and the depth is $D$

Philippe *et al.*: Elastic target characterization in shallow water

a)



b)
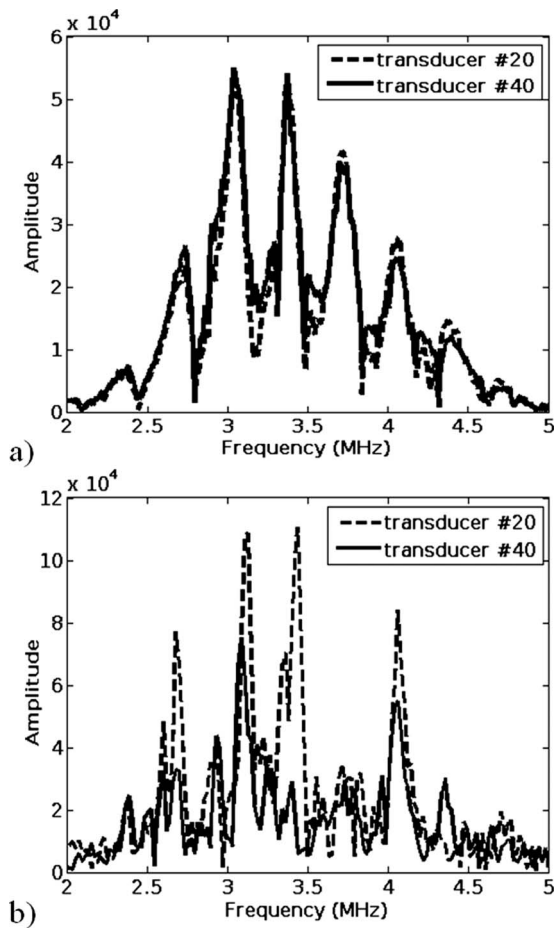
FIG. 4. Monostatic frequency response of 3 mm steel sphere for two transducers (a) in free space and (b) in a 28.1-mm-deep water waveguide.



FIG. 5. First three singular values of a 3 mm steel sphere in a 28.1-mm-deep waveguide at distance $R=575$ mm. The experimental data (continuous line) are obtained in the waveguide. The theoretical curves (dash-dotted line) are computed in a free space configuration (Ref. 19) with a virtual SRA corresponding to three reflections at the surface and the bottom.

$=28.1$ mm (65$\lambda$). The guide's width is 60 cm which is sufficiently large to avoid lateral reflections. The distance between the array and the targets is $R=575$ mm, i.e., 1340$\lambda$.

These small scale experiments give an idea of what would happen for at sea experiments. For a SRA working at 12.5 kHz, the equivalent waveguide would be 160 m long and 8 m deep.

## B. Resonant scatterer

### 1. Backscattering form function

Two examples of the monostatic frequency response from a 3-mm-diameter steel sphere in free space are plotted in Fig. 4(a). As $2a > \lambda R/D$, the sphere can be considered as a large object. It clearly appears that the backscattered signal weakly depends on the transducer's position and the oscillations are related to the sphere resonances. In order to provide a comparison, two monostatic responses in the waveguide are plotted in Fig. 4(b). In free space, the backscattered response is directly proportional to the target backscattering form function while in the waveguide, the response is much more complex and strongly depends on the transducer position. These effects are due to the complex interference pattern generated by the multiple reflections at the waveguide boundaries.

### 2. Form function and singular values

The scatterer is a 3-mm-diameter steel sphere in the waveguide at a depth of 13 mm. The first three singular values obtained in the waveguide are plotted in Fig. 5 versus frequency. These curves are compared to the theoretical ones obtained in a free space configuration [19] accounting for the corresponding virtual array. For the computation, the size of the virtual SRA, $D'$, is chosen such as $D'=2R \sin(\theta_{max})$ with $\theta_{max}=20°$ corresponding to a virtual aperture seven times larger than the real array aperture.

This result shows that DORT facilitates the extraction of the backscattering signature and its second derivative without frequency distortion. Even more, the waveguide, by a virtual aperture effect, increases the singular values, leading to a better target, characterization in noisy environment. This effect is particularly significant with the second singular value which is proportional to $\sin^3(\theta_{max})$.

The first two singular vectors are numerically back-propagated with the range-dependent acoustic model (RAM) numerical simulation [23]. To that end, the RAM configuration takes into account the waveguide geometry, in particular, the weak bottom slope of 0.4°. At one frequency, the experimental singular vector is phase conjugated and each element of the vector is the phase and amplitude excitation for the elements of the simulated array. After numerical propagation, the acoustic field value is stored in computer memory. The simulation is repeated for several frequencies between 2 and 5 MHz. The averaged field around the focus is plotted in Fig. 6 in logarithmic scale.

As in free space the first and the second singular values lead, respectively, to symmetric and antisymmetric focusing. However, this is only true in the vicinity of the sphere because unlike in free space, far from the focus, the focal spot symmetry is lost due to interaction with the boundaries. The focal spot is 1.4 mm wide; thus the virtual array obtained is at least six times larger than the real one, thanks to the re-
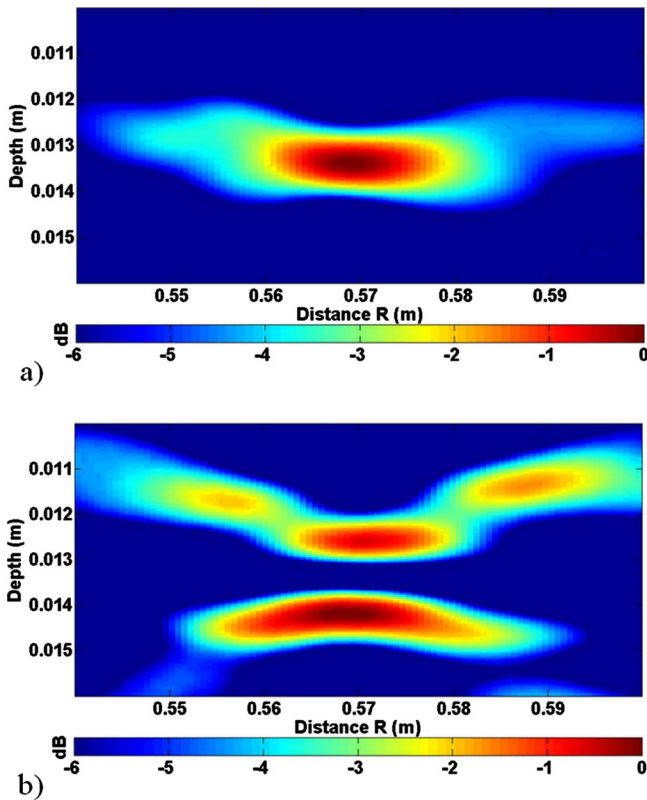
FIG. 6. (Color online) Backpropagation with RAM code of the first two singular vectors. (a) and (b) represent the acoustical energy averaged over all frequencies between 2 and 5 MHz in logarithmic scale.

flections on the interfaces of the waveguide. This is in agreement with the virtual aperture $D' = 197$ mm introduced previously.

## C. Separation of two elastic spheres

The following experiment illustrates two aspects of the DORT method: the detection of two targets at the same range and the extraction of their form functions. The experiment was performed in the same waveguide as in the previous sections with two steel spheres of radii differing by 5%. This radius mismatch induces a 5% difference in the resonance frequencies. The distance between the two spheres is 10 mm which is much larger than $D/\sin(\theta_{max})$, so that, according to the results of Sec. II B, the responses of the two spheres weakly interact.

The first four singular values as a function of the frequency are displayed in Fig. 7. There is no simple way to associate a singular value with a target, in particular, the first singular value may not correspond to the same target at all frequencies. One target may have the highest reflectivity at one frequency (for example, at a resonance frequency) while the other has the highest reflectivity at another frequency. This is why here the first two singular values corresponding to the two backscattering form functions of the spheres are intertwined due to the slight radius mismatch. The target corresponding to the first singular value is either the 3 mm sphere or the 3.15 mm sphere. The frequencies where the switchings occur are emphasized in Figs. 8(a) and 9(a) by vertical lines. The two backscattering form functions can be
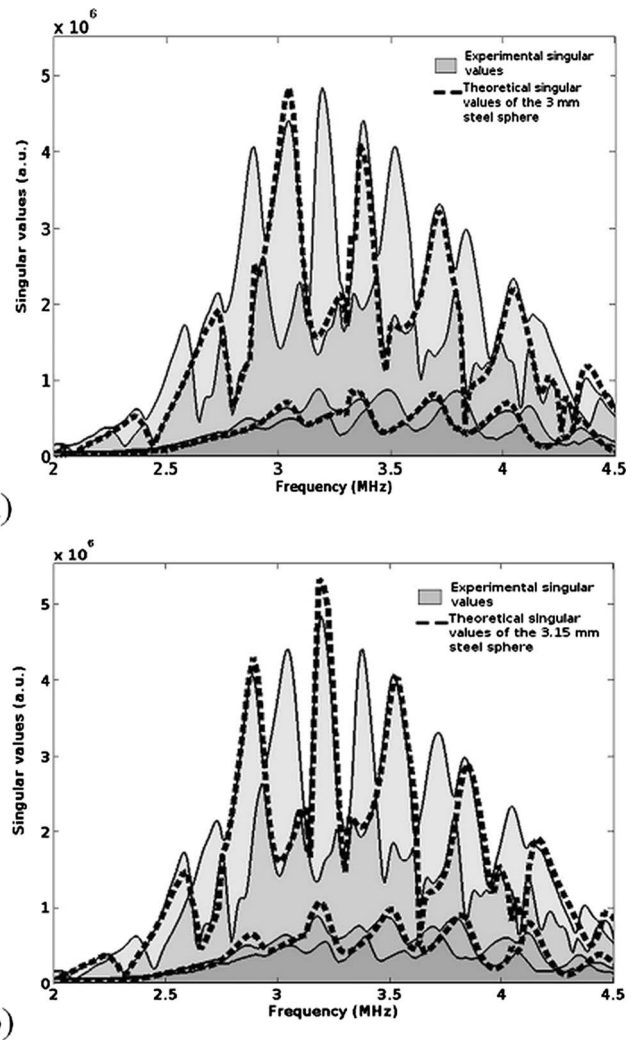


FIG. 7. Two different spheres in a waveguide: comparison between the first four experimental singular values and the first two theoretical singular values of the (a) 3 mm steel sphere and (b) 3.15 mm steel sphere.

assigned to their corresponding spheres by comparing the singular value to the theoretical backscattering form function of each sphere taken alone. Indeed, as shown in Sec. II B, for distant scatterers, there is one singular value associated with each scatterer. Each singular value is the one obtained at the same conditions but without the other scatterer. Similar effects occur for the other two singular values.

The backpropagation of the singular vectors as a function of frequency is shown in Figs. 8 and 9 and confirms this result. The backpropagated field associated with the first singular value focuses at the depth of the sphere with the highest backscattering form function. The second singular vector focuses at the position of the other sphere. The same effect occurs when the third singular vector is backpropagated; the dipolar focal spot is centered on the strongest target. The switches from one sphere position to the other correspond to singular value crossings that are shown by vertical lines in Fig. 9. Thus the backpropagation provides a means to reconstruct the frequency dependence of the backscattering form function for each target.
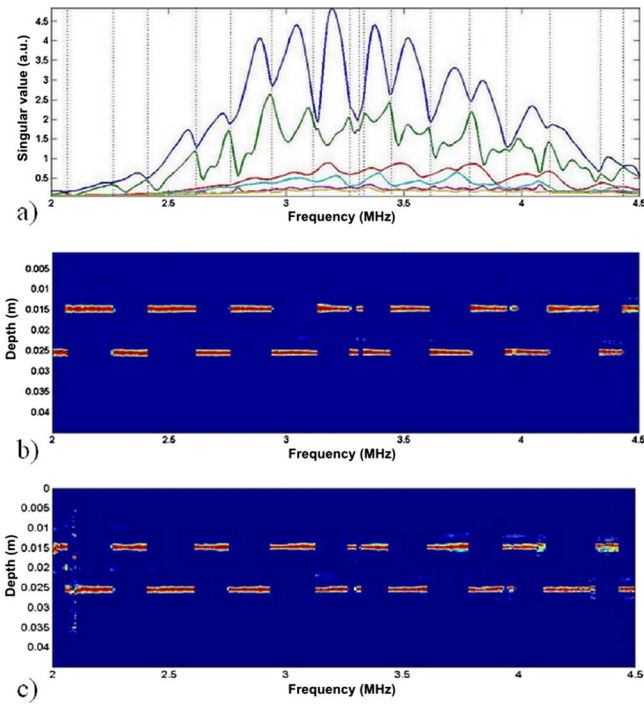
FIG. 8. (Color online) (a) Measured singular values of the two spheres as a function of frequency. A vertical line designates a frequency where a switch in the relative strength of the targets occurs. (b) Backpropagation with RAM code of the first eigenvector as a function of frequency and depth at a range of 575 mm. (c) Backpropagation with RAM code of the second eigenvector at the same distance.

## IV. CONCLUSION

In this paper, the authors have presented a theoretical and experimental study of the eigenvectors of the time reversal operator for a scatterer in shallow water with a modal approach to wave propagation. By using a normal mode expansion and introducing the form function of an isotropic target within the paraxial approximation, the length $\Lambda = \lambda/2 \sin(\theta_{max})$ was demonstrated to correspond to the Rayleigh criterion. Indeed, it was shown that two targets at the
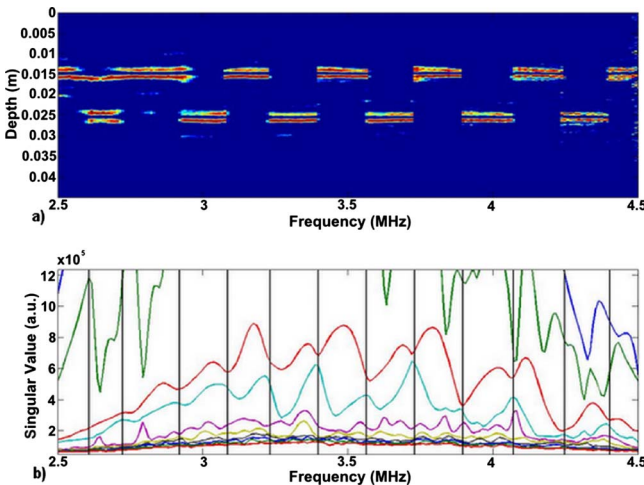


FIG. 9. (Color online) (a) Backpropagation with RAM code of the third eigenvector as a function of frequency and depth at a range of 575 mm. The focusing is antisymmetric with respect to the scatterer center as predicted by theory. (b) Zoom on the third and fourth singular values as a function of frequency.

same range are weakly coupled when the depth difference is larger than $\Lambda$ and that when one target is at least $\Lambda$ away from the boundaries, the frequency dependence of the first singular value is nearly identical to the backscattering target signature. Moreover it was shown that the second singular value is proportional to the second derivative of the angular form function. The second singular value is an interesting complementary identification parameter especially because guided propagation enhances it by a factor $N_{reflex}^3$ which is the number of reflections to the power 3.

The small scale experiments presented in this paper are in good agreement with the theory. The extended targets used were steel spheres, each having several associated singular values. Their backscattered frequency signatures were successfully extracted from the impulse response matrix without any evaluation of the waveguide parameters. The DORT method is able to detect, separate, and discriminate between two spheres with diameters that only differ by 5%. Such precision is very promising for further at sea experiments.

Hence it was shown that the DORT method enables target characterization without the need of precise knowledge of the waveguide when the target is at least $\Lambda$ away from any other element of the medium.

Furthermore, additional knowledge can be obtained when an accurate numerical model of the waveguide is available: localization of the targets is possible and backpropagation of the singular vectors provides a means to associate a form function with a target without any ambiguity.

## APPENDIX A: FIRST SINGULAR VALUE FOR AN ISOTROPIC SCATTERER IN A WAVEGUIDE

The singular values $\sigma_1$ is given by

$$
\begin{aligned}
\sigma_1 &= \frac{|S(0)|}{4\pi R D k_0 \delta} \sum_{m=0}^{M-1} \sin^2(k_{zm} z_s) \\
&= \frac{|S(0)|}{4\pi R D k_0 \delta} \sum_{m=0}^{M-1} \frac{1 - \cos(2k_{zm} z_s)}{2} \\
&= \frac{|S(0)|}{8\pi R D k_0 \delta} \left[ M - \Re e \left( \sum_{m=0}^{M-1} e^{i2(m+1/2)\pi/D z_s} \right) \right] \\
&= \frac{|S(0)|}{8\pi R D k_0 \delta} \left[ M - \Re e \left( e^{i(\pi/D)z_s} \sum_{m=0}^{M-1} (e^{i2(\pi/D)z_s})^m \right) \right].
\end{aligned}
\tag{A1}
$$

Moreover, the geometric series with common ratio $e^{i2(\pi/D)z_s}$ has the following exact solution:

$$
\sum_{m=0}^{M-1} (e^{i2(\pi/D)z_s})^m = \frac{1 - e^{i2(\pi/D)Mz_s}}{1 - e^{i2(\pi/D)z_s}}.
\tag{A2}
$$

Thus Eq. (1) becomes

$$\sigma_1 = \frac{|S(0)|}{8\pi R D k_0 \delta}\left[ M - \cos\left(\frac{\pi M z_s}{D}\right)\frac{\sin\left(\frac{\pi M z_s}{D}\right)}{\sin\left(\frac{\pi z_s}{D}\right)}\right]. \quad \text{(A3)}$$

For convenience the function $f_M$ is defined as follows:

$$f_M(\xi) = \left(\cos(\pi M \xi)\frac{\sin(\pi M \xi)}{\sin(\pi \xi)}\right). \quad \text{(A4)}$$

The expression of the first singular value can then be concisely written as

$$\sigma_1 = \frac{|S(0)|}{8\pi R D k_0 \delta}\left[ M - f_M\left(\frac{z_s}{D}\right)\right]. \quad \text{(A5)}$$

## APPENDIX B: DERIVATION OF THE COUPLING TERM FOR TWO SCATTERERS

At the same range, the inner product between $\mathbf{h}_{s1}$ and $\mathbf{h}_{s2}$ is given by

$$^\dagger\mathbf{h}_{s2}\mathbf{h}_{s1} = \frac{1}{\delta\rho 8\pi R}\sum_{m=0}^{\infty}\Psi_m(z_{s1})\Psi_m(z_{s2}). \quad \text{(B1)}$$

Again we consider a Pekeris waveguide. Moreover, assuming that the array is only sensitive to small incident angles, the inner product can be approximated by

$$^\dagger\mathbf{h}_{s2}\mathbf{h}_{s1} \approx \frac{1}{\delta 4\pi R D k_0}\sum_{m=0}^{M-1}\sin(k_{zm}z_{s1})\sin(k_{zm}z_{s2}). \quad \text{(B2)}$$

Using a well-known trigonometric relation, it becomes

$$^\dagger\mathbf{h}_{s2}\mathbf{h}_{s1} \approx \frac{1}{\delta 8\pi R D k_0}\sum_{m=0}^{M-1}\left[\cos(k_{zm}[z_{s1} - z_{s2}])\right.$$
$$\left. - \cos(k_{zm}[z_{s1} + z_{s2}])\right]. \quad \text{(B3)}$$

The sum of the cosines is calculated as in Appendix A.

$$^\dagger\mathbf{h}_{s2}\mathbf{h}_{s1} \approx \frac{1}{\delta\rho 8\pi R D k_0}\left[f_M\left(\frac{z_1 + z_2}{2D}\right) - f_M\left(\frac{z_1 - z_2}{2D}\right)\right]. \quad \text{(B4)}$$

## APPENDIX C: DERIVATION OF THE COUPLING TERM BETWEEN $h_s$ AND $\partial_z h_s$

Here we want to compute the norm of the first derivative of $\mathbf{h}$ over $z$ and the inner product between $\mathbf{h}_s$ and $\partial_z\mathbf{h}_s$, i.e.,

$$\|\partial_z\mathbf{h}_s\|^2 = \frac{1}{\delta\rho 8\pi R}\sum_{m=0}^{\infty}\frac{[\partial_z\Psi_m(z_s)]^2}{k_{rm}}, \quad \text{(C1)}$$

$$^\dagger\mathbf{h}_s\partial_z\mathbf{h}_s = \frac{1}{\delta\rho 8\pi R}\sum_{m=0}^{\infty}\frac{\Psi_m(z_s)\partial_z\Psi_m(z_s)}{k_{rm}}. \quad \text{(C2)}$$

Assuming a perfect waveguide and a cutoff for the mode summation, Eqs. (C1) and (C2) can be written as

$$\|\partial_z\mathbf{h}_s\|^2 = \frac{1}{\delta 4\pi R D k_0}\sum_{m=0}^{M-1}k_{zm}^2\cos^2(k_{zm}z_s), \quad \text{(C3)}$$

$$^\dagger\mathbf{h}_s\partial_z\mathbf{h}_s = \frac{1}{\delta 4\pi R D k_0}\sum_{m=0}^{M-1}k_{zm}\sin(k_{zm}z_s)\cos(k_{zm}z_s). \quad \text{(C4)}$$

These two expressions can be worked out using the first and second derivatives of $f_M$. Indeed,

$$^\dagger\mathbf{h}_s\partial_z\mathbf{h}_s = \frac{1}{\delta 4\pi R D k_0}\frac{1}{2D}f_M'\left(\frac{z_s}{D}\right), \quad \text{(C5)}$$

and

$$\|\partial_z\mathbf{h}_s\|^2 = \frac{1}{\delta 8\pi R D k_0}\left(\frac{(4M^3 - M)\pi^2}{12D^2} + \frac{f_M''\left(\frac{z_s}{D}\right)}{4D^2}\right). \quad \text{(C6)}$$

$$\partial_\xi f_M(\xi) = \left(\frac{2M\sin(\pi\xi)\cos(2\pi M\xi) - \cos(\pi\xi)\sin(2\pi M\xi)}{2\sin^2(\pi\xi)}\right), \quad \text{(C7)}$$

$$\Sigma = \frac{f_M'\left(\frac{z_s}{D}\right)}{\sqrt{\frac{M - f_M\left(\frac{z_s}{D}\right)}{4}\left[\frac{(4M^3 - M)\pi^2}{3} + f_M''\left(\frac{z_s}{D}\right)\right]}}. \quad \text{(C8)}$$

## APPENDIX D: ENHANCEMENT OF THE SINGULAR VALUES DUE TO THE WAVEGUIDE

In free space, the first singular value is easily calculated:

$$\sigma_1^{\text{free}} = S(0)\|h_{\text{free}}\|^2 \quad \text{(D1)}$$

with Eq. (4) and $G(z,z_s,r_s-r_i)=(1/4\pi)(e^{-ikR}/R)$ the first singular value in free space becomes

$$\sigma_1^{\text{free}} = \frac{S(0)D}{\delta(4\pi R)^2}, \quad \text{(D2)}$$

where $D$ is the array aperture and $\delta$ is the array pitch.

In the same manner the second singular value is

$$\sigma_2^{\text{free}} = \frac{S''(0)\|\partial_z h_{\text{free}}\|^2}{k_0^2} \approx \frac{S''(0)D^3}{48\delta R^4\lambda^2 k_0^2}. \quad \text{(D3)}$$

It was shown in Sec. II C that in a waveguide, the expression of the singular values is

$$\sigma_1^{\text{guide}} = \frac{|S(0)|M}{8\pi R k_0 D\delta} \quad \text{and} \quad \sigma_2^{\text{guide}} = \frac{S''(0)\|\partial_z h_{\text{guide}}\|^2}{2k_0}.$$

As a consequence

$$\frac{\sigma_1^{\text{guide}}}{\sigma_1^{\text{free}}} = \frac{|S(0)|M}{8\pi R k_0 D\delta} \times \frac{\delta(4\pi R)^2}{|S(0)|D}$$

with

$$M = \frac{N_{\text{reflex}} D^2}{\lambda R}. \tag{D4}$$

The ratio becomes $\sigma_1^{\text{guide}} / \sigma_1^{\text{free}} = N_{\text{reflex}}$.

Keeping only the $M^3$ term, Eq. (C6) becomes

$$\sigma_2^{\text{guide}} = \frac{S''(0) M^3 \lambda}{48 \delta R D^3 k_0^2} = \frac{S''(0)(2 \sin \theta_d)^3}{48 \delta R k_0^2 \lambda^2}, \tag{D5}$$

with $M = 2 \sin \theta_d D / \lambda$.

$$\frac{\sigma_2^{\text{guide}}}{\sigma_2^{\text{free}}} = \frac{(2 \sin \theta_d)^3 R^3}{D^3} = N_{\text{reflex}}^3. \tag{D6}$$

[1]R. H. Hackman and G. S. Sammelmann, "Multiple scattering analysis for a target in an oceanic waveguide," J. Acoust. Soc. Am. **84**, 1813–1825 (1988).

[2]F. Ingenito, "Scattering from an object in a stratified medium," J. Acoust. Soc. Am. **82**, 2051–2059 (1987).

[3]P. Mignerey and S. Finette, "Multichannel deconvolution of an acoustic transient in an oceanic waveguide," J. Acoust. Soc. Am. **92**, 351–364 (1992).

[4]S. Finette, P. Mignerey, J. Smith III, and C. Richmond, "Broadband source signature extraction using a vertical array," J. Acoust. Soc. Am. **94**, 309–318 (1993).

[5]T. C. Yang and T. W. Yates, "Scattering from an object in a stratified medium. II. Extraction of scattered signature," J. Acoust. Soc. Am. **96**, 1020 (1994).

[6]W. A. Kuperman, W. S. Hodgkiss, H. C. Song, T. Akal, C. Ferla, and D. R. Jackson, "Phase conjugation in the ocean: Experimental demonstration of an acoustic time-reversal mirror," J. Acoust. Soc. Am. **103**, 25–40 (1998).

[7]W. S. Hodgkiss, H. C. Song, W. A. Kuperman, T. Akal, C. Ferla, and D. R. Jackson, "A long-range and variable focus phase conjugation experiment in shallow water," J. Acoust. Soc. Am. **105**, 1597–1604 (1998).

[8]P. Roux and M. Fink, "Time reversal in a waveguide: Study of the temporal and spatial focusing," J. Acoust. Soc. Am. **107**, 2418–2429 (2000).

[9]N. Mordant, C. Prada, and M. Fink, "Highly resolved detection and selective focusing in a waveguide using the D.O.R.T. method," J. Acoust. Soc. Am. **105**, 2634–2642 (1999).

[10]B. Pinçon and L. Ramdani, "Selective focusing on small scatterers in acoustic waveguides using time reversal mirrors," Inverse Probl. **23**, 1–25 (2007).

[11]T. Folégot, C. Prada, and M. Fink, "Resolution enhancement and separation of reverberation from target echo with the time reversal operator decomposition," J. Acoust. Soc. Am. **113**, 3155–3160 (2003).

[12]J. F. Lingevitch, H. C. Song, and W. A. Kuperman, "Time reversed reverberation focusing in a waveguide," J. Acoust. Soc. Am. **111**, 2609–2614 (2001).

[13]H. C. Song, W. S. Hodgkiss, W. A. Kuperman, P. Roux, T. Akal, and M. Stevenson, "Experimental demonstration of adaptive reverberation nulling using time reversal," J. Acoust. Soc. Am. **118**, 1381–1387 (2005).

[14]C. Prada, J. De Rosny, D. Clorennec, J. G. Minonzio, A. Aubry, M. Fink, L. Bernière, S. Hibral, P. Billand, and T. Folégot, "Experimental detection and focusing in shallow water by decomposition of the time reversal operator," J. Acoust. Soc. Am. **122**, 768–761 (2007).

[15]C. F. Gaumond, D. M. Fromm, J. F. Lingevitch, R. Menis, G. F. Edelmann, D. C. Calvo, and E. Kim, "Demonstration at sea of the decomposition-of-the-time-reversal-operator technique," J. Acoust. Soc. Am. **119**, 976–990 (2006).

[16]D. H. Chambers and A. K. Gautesen, "Time reversal for a single spherical scatterer," J. Acoust. Soc. Am. **109**, 2616–2624 (2001).

[17]D. H. Chambers, "Analysis of the time-reversal operator for scatterers of finite size," J. Acoust. Soc. Am. **112**, 411–419 (2002).

[18]J. G. Minonzio, C. Prada, D. Chambers, D. Clorennec, and M. Fink, "Characterization of subwavelength elastic cylinders with the decomposition of the time-reversal operator: Theory and experiment," J. Acoust. Soc. Am. **117**, 789–798 (2005).

[19]J. G. Minonzio, F. D. Philippe, C. Prada, and M. Fink, "Characterization of an elastic cylinder and an elastic sphere with the time-reversal operator: application to the sub-resolution limit," Inverse Probl. **24**, 025014 (2008).

[20]G. C. Gaunaurd and H. Huang, "Acoustic scattering by a spherical body near a plane boundary," J. Acoust. Soc. Am. **96**, 2526–2536 (1994).

[21]F. B. Jensen, W. A. Kuperman, M. B. Porter, and H. Schmidt, *Computational Ocean Acoustics* (American Institute of Physics, New York, 1994), Chap. 2, pp. 123–127.

[22]J. G. Minonzio, C. Prada, A. Aubry, and M. Fink, "Multiple scattering between two elastic cylinders and invariants of the time-reversal operator: Theory and experiments," J. Acoust. Soc. Am. **102**, 875–883 (2006).

[23]M. D. Collins, "A split-step Padé solution for the parabolic equation method," J. Acoust. Soc. Am. **93**, 1736–1742 (1993).